Implantable hydrogel embedded dark-gold nanoswitch as a theranostic probe to sense and overcome cancer multidrug resistance

João Conde[a,b,1], Nuria Oliva[a], and Natalie Artzi[a,c,1]

[a]Institute for Medical Engineering and Science, Massachusetts Institute of Technology, Cambridge, MA 02139; [b]School of Engineering and Materials Science, Queen Mary University of London, London E1 4NS, United Kingdom; and [c]Department of Anesthesiology, Brigham and Women's Hospital, Harvard Medical School, Boston, MA 02115

Edited by Alexis T. Bell, University of California, Berkeley, CA, and approved February 4, 2015 (received for review November 5, 2014)

Multidrug resistance (MDR) in cancer cells is a substantial limitation to the success of chemotherapy. Here, we describe facile means to overcome resistance by silencing the multidrug resistance protein 1 (*MRP1*), before chemotherapeutic drug delivery in vivo with a single local application. Our platform contains hydrogel embedded with dark-gold nanoparticles modified with 5-fluorouracil (5-FU)-intercalated nanobeacons that serve as an ON/OFF molecular nanoswitch triggered by the increased *MRP1* expression within the tumor tissue microenvironment. This nanoswitch can sense and overcome MDR prior to local drug release. The nanobeacons comprise a 5-FU intercalated DNA hairpin, which is labeled with a near-infrared (NIR) dye and a dark-quencher. The nanobeacons are designed to open and release the intercalated drug only upon hybridization of the DNA hairpin to a complementary target, an event that restores fluorescence emission due to nanobeacons conformational reorganization. Despite the cross-resistance to 5-FU, more than 90% tumor reduction is achieved in vivo in a triple-negative breast cancer model following 80% *MRP1* silencing compared with the continuous tumor growth following only drug or nanobeacon administration. Our approach can be applied to reverse cross-resistance to other chemotherapeutic drugs and restore treatment efficacy. As a universal nanotheranostic probe, this platform can pave the way to early cancer detection and treatment.

hydrogels | gold nanobeacons | theranostics | breast cancer | multidrug resistance

Multidrug resistance (MDR) in cancer is a phenomenon whereby cancer cells gain the capacity to develop cross-resistance and survive a variety of structurally and functionally unrelated drugs (1). The most common MDR mechanisms occur by the expression of one or more energy-dependent transporters, which can result in an increased efflux of the cytotoxic drugs from the cancer cells, thus lowering their intracellular concentrations (2). The phosphoglycoprotein multidrug resistance protein 1 (*MRP1* or ABCC1) is often associated with resistance to a broad spectrum of anticancer drugs and belongs to the ATP-binding cassette (ABC) superfamily of proteins as energy-dependent efflux pumps (3). The ABC transporters are essential not only to breast cancer MDR but also to other types of cancer, such as non–small cell lung cancer, lung cancer, and rectal cancer (4). In fact, increased ABC expression levels have been shown to correlate with decreased response to various chemotherapy drugs [such as 5-fluorouracil (5-FU)] and a decrease in overall survival (5). 5-FU is widely used in cancer therapy as it has the capacity to interfere with nucleoside metabolism and result in DNA and RNA synthesis disorders and dysfunction, leading to cytotoxicity and cell death. Based on the American Cancer Society guidelines, 5-FU is used to treat a range of cancerous diseases, including colon and rectal cancer; breast cancer; gastrointestinal cancers including anal, esophageal, pancreas, and gastric (stomach); head and neck cancer; and ovarian cancer. For decades, 5-FU has been used in combination with other antineoplastic agents or as a single agent in the adjuvant and palliative treatment of advanced breast cancer (6). Nevertheless, the overall response to this drug remains only 15% due to resistance mechanisms (7). Hence, despite the remarkable progress in chemotherapeutic drug development in the last decade, ∼70% of cancer patients do not respond to chemotherapy and have a 5-y survival rate of 10–30% (8). Consequently, new platforms that are able to improve antitumor efficacy are urgently needed.

The development of nanoscale devices has provided major breakthroughs in cancer diagnostic and therapy (9–13), especially in drug delivery (14, 15). Because nanoparticles are excellent tumor-targeting vehicles due to enhanced permeability and retention (EPR) in the tumor microenvironment (having defective vasculature and poor lymphatic drainage) (16, 17), they can be harnessed to alter MDR mechanisms. Indeed nanomaterials have been used to help overcome MDR by increasing drug retention in cancer cells and hamper cancer progression (7, 18–20). Nevertheless, a platform that senses and inhibits MDR gene expression followed by selective drug release has not been reported yet.

Here we developed a universal nanodevice able to sense specific gene sequence, silence it, and release a chemotherapeutic drug, while reporting on these events. A bioresponsive hydrogel-nanoprobe that locally senses and inhibits the expression of the *MRP1*, followed by subsequent release of 5-FU drug to resistant triple-negative breast cancer cells (TNBC), was developed. Breast cancer was chosen as a model because it can benefit from local non-invasive administration of an injectable hydrogel. TNBC accounts for 15–20% of all breast cancers, and it represents the most aggressive subtype with a direct prognosis. TNBCs are characterized

Significance

The integration of biomaterials science, innovative imaging, and cancer biology now enables the design of smart responsive material platforms for cancer theranostics. We show herein that our developed nanovehicle is able to sense and silence a multidrug resistance gene based on its expression in the tumor microenvironment, followed by local chemotherapeutic drug release, with a significant tumor regression not achieved otherwise. This ON/OFF molecular nanoswitch approach can be used to reverse the resistance to many other chemotherapeutic drugs and can serve as a universal gene therapy and drug delivery vehicle for cancer therapy. This disease-responsive platform can revolutionize clinical outcome and cancer patients' point of care.

Author contributions: J.C. and N.A. designed research; J.C. and N.O. performed research; J.C. and N.O. contributed new reagents/analytic tools; J.C., N.O., and N.A. analyzed data; and J.C., N.O., and N.A. wrote the paper.

The authors declare no conflict of interest.

This article is a PNAS Direct Submission.

[1]To whom correspondence may be addressed. Email: jdconde@mit.edu or nartzi@mit.edu.

This article contains supporting information online at www.pnas.org/lookup/suppl/doi:10.1073/pnas.1421229112/-/DCSupplemental.

by resistance to apoptosis, aggressive cellular proliferation, migration and invasion, and currently lack molecular markers and effective targeted therapy. TNBC patients suffer from poor survival rates and limited efficacy of neoadjuvant chemotherapy, as tumors from such patients are characterized by overexpression of specific genes involved in drug-desensitizing mechanisms (21). We now show that smart bioresponsive hydrogel-nanoprobes are able to reduce 5-FU drug-resistant tumors by 90% 14 d after hydrogel implantation in breast cancer tumor-bearing mice by silencing more than 80% of *MRP1* expression before drug release. This approach can be applied to improve treatment efficacy using other chemotherapeutic drugs for a range of solid tumors.

Results and Discussion

Bioresponsive Dark-Gold Nanoswitch Design. Our nanoprobe encompasses a gold nanoparticle (AuNP) core decorated with a thiol-DNA hairpin labeled with a near-infrared (NIR) dye (intercalated with a chemotherapeutic drug, 5-FU) and a thiol-DNA oligo labeled with a Black-Hole dark quencher (Fig. 1*A*), which is used as a two-pair FRET/nanosurface energy transfer (NSET) donor quencher nanoconjugate for universal cancer gene therapy and drug delivery. Polyethylene glycol (PEG) is also used as a spacer between the hairpins, increasing their nanostructure stability in biological medium (22–24) (see *SI Appendix*, Fig. S1 for PEG optimization and quantification). Thiol-DNA oligo labeled with a dark quencher is used to quench nanobeacon fluorescence. Under hairpin configuration, the proximity of the NIR dye (Quasar 705) to the dark quencher (BHQ2) leads to fluorescence quenching. Hybridization of the DNA hairpin to a complementary target (i.e., *MRP1* mRNA) restores fluorescence emission due to the gold nanobeacon conformational reorganization that causes the fluorophore and the quencher to part from each other, yielding a quantitative response.

The mechanism of mRNA knockdown in this study is based on antisense DNA technology (25). This method was used to inhibit or down-regulate the production of *MRP1* protein by using antisense DNA oligonucleotides, the DNA molecular beacon anti-*MRP1*, which precisely complements the *MRP1* mRNA target sequence present in the cell. These molecular beacons have the ability to interlock or hybridize with the target *MRP1* mRNA (blocking specific translation initiation signals of *MRP1* gene), thus inhibiting the translation of the target protein. Oligomers sequences and 2D structures of the beacons at 37 °C are depicted in *SI Appendix*, Table S1 and Fig. S2*A*, respectively.

The release of the 5-FU drug is designed to occur only when DNA hairpin hybridizes with the complementary mRNA target inside the cell and can be tracked fluorescently once the distance between 5-FU and the gold core increases upon drug release. The 5-FU wedge between bases along the dsDNA part of the nanobeacon. The drug covalently binds to DNA in different sites producing intrastrand cross-links, preventing the polymerase and other DNA binding proteins from functioning properly, which results in DNA synthesis, inhibition of transcription, and induction of mutations. The choice of fluorophores and quenchers enabled the gold nanobeacon with BHQ2 dark quencher, which extends to the near-infrared emission wavelengths, to overlap with the absorbance range of the Quasar 705 fluorophore, and the surface plasmon resonance (SPR) profile from gold nanobeacon to overlay the absorbance wavelength from the 5-FU at 450 nm (*SI Appendix*, Fig. S2*B*). The BHQ2 group functioned as quencher for the Q705 (donor 1) and the AuNPs functioned as the quenchers for the 5-FU (donor 2). The NIR dye and dark quencher, Quasar 705nm (Q705) and BHQ2 (26) (Black Hole Quencher-2 with a strong absorption from 599 to 670 nm), were chosen to enable efficient quenching in the nanobeacon basal state with restored fluorescence upon conjugation to the appropriate target. The fluorescence emission from the 5-FU (Emi = 450 nm) is efficiently quenched by the ∼14-nm AuNP due to the NSET effect (27). This NSET effect provides the dark-gold nanobeacons with the ability to serve as an on/off switch. This capability is particularly useful for tracking drug release in response to a specific gene expression within the tumor microenvironment. These events, binding to a target and the resulting drug release, are each reported by fluorescence emission in a defined wavelength.

In addition to designing an anti-*MRP1* nanobeacon that detects and inhibits *MRP1* mRNA, anti-Luc nanobeacons (that hybridize with luciferase mRNA and release the drug without targeting *MRP1*) and nonsense nanobeacons (that do not hybridize with any target) were developed as controls (*SI Appendix*, Fig. S2*A* and Table S1).

Transmission electron microscopy (TEM) images of the dark-gold nanobeacons loaded with 5-FU showed an average diameter ± SD of the gold core of 13.8 ± 3.4 nm (*SI Appendix*, Fig. S2*C*). The final Q705 DNA hairpin:NP and BHQ2 oligo:NP ratios were approximately 30:1 and 24:1, respectively. The ratio for 5-FU:NP was 100:1 (*SI Appendix*, Table S2). The mean particle diameter ± SD of dark-gold nanobeacons is 25.5 ± 1.2 nm without 5-FU and 31.1 ± 0.5 nm loaded with 5-FU, with an SPR peak around 548–550 nm as measured by dynamic light scattering (DLS) and UV-Vis extinction profiles, respectively (Fig. 1*D* and *SI Appendix*, Table S2).

The fluorescence is OFF when the hairpin-DNA-Q705 is closed (i.e., no hybridization with the complementary target), inhibiting 5-FU release (Fig. 1*A*). The fluorescence is ON when the hairpin-DNA-Q705 hybridizes with a complementary target and an increase in Q705 emission occurs, with a concomitant 5-FU release and increase in the drug emission (Fig. 1*A*). It is worth noting that the fluorescence emission intensity of Q705-labeled DNA oligo is significantly decreased following their conjugation to the dark-gold nanoparticles. The binding between the Q705-labeled DNA oligo and the dark-gold nanoparticles occurs by a direct quasi-covalent bond between the thiol group on the 5′ end of the oligo and the gold surface by ligand-exchange between the citrate groups on the surface of the AuNPs and thiol groups. When the concentration of Q705-labeled DNA oligo was fixed at 0.5 μM, the increase in dark-gold nanobeacons concentration from 0 to 10 nM in the reaction mixture resulted in a significant increase in Q705 fluorescence quenching (Fig. 1*B*), demonstrating the presence of NSET between the Q705 groups and the dark-gold nanobeacons. These experimental data showed a quenching efficiency of nearly 99% when the concentration of dark-gold nanobeacons reached 1 nM, whereas it was nearly 100% when the concentration of AuNPs reached 2.5 nM. These data confirm that the combination of BHQ2 oligo and attachment to the surface of gold nanobeacons provides powerful fluorescence quenching for Q705 emission. The same phenomenon occurs for 5-FU loading on dark-gold nanobeacons (Fig. 1*C*). When 1 mM 5-FU was loaded on 2.5 nM dark-gold nanobeacons, the fluorescence emission spectra of 5-FU after incubation in phosphate buffer (pH 7.0, 10 mM) for different periods of time (0–120 min) confirmed a significant increase in 5-FU fluorescence quenching (Fig. 1*C*). This phenomenon indeed indicated the formation of dark-gold nanobeacons loaded with 5-FU. Conversely, the Q705 emission can be restored after hybridization with the complementary ssDNA target. Increasing amounts of complementary target results in elevated emission form the Q705 dye until reaching a plateau at 1 μM of target (Fig. 1*D*) and in 5-FU release, with nearly complete drug release at 1 μM of target (Fig. 1*E*). We studied the release kinetics of the intercalated drug following fluorescence of the 5-FU that was measured for 75 min following addition of 1 μM of target and compared it with the fluorescence of the Q705 (*SI Appendix*, Fig. S3). As expected, the kinetics of the 5-FU release follows that of nanobeacons opening subsequent to the hybridization of a fully complementary target.

The stability of dark-gold nanobeacons loaded with 5-FU toward variations in temperature, pH, DNase, and glutathione (GSH) concentration was also evaluated (*SI Appendix*, Figs. S4–S7). These data confirm the stability of the dark-gold nanobeacons loaded with 5-FU at room and physiological (37 °C) temperatures (*SI Appendix*, Fig. S4) and in a wide pH range (4.5–8) (*SI Appendix*, Fig. S5), as well as intracellular concentrations of GSH (*SI Appendix*, Fig. S6) and DNase (*SI Appendix*, Fig. S7).

***MRP1* Triggered 5-FU Release in Vitro.** To test the ability of dark-gold nanobeacons loaded with 5-FU to overcome MDR, nanobeacons intracellular uptake and trafficking was examined using a 5-FU–resistant MDA-MB-231 breast cancer cell line obtained by continuous culturing of parental MDA-MB-231 cells in a 0.05-mg/mL dose of 5-FU. Drug resistance was confirmed by the absence of cell death using the [3-(4,5-dimethylthiazol-2-yl)-2,5-diphenyltetrazoliumbromide] (MTT) assay

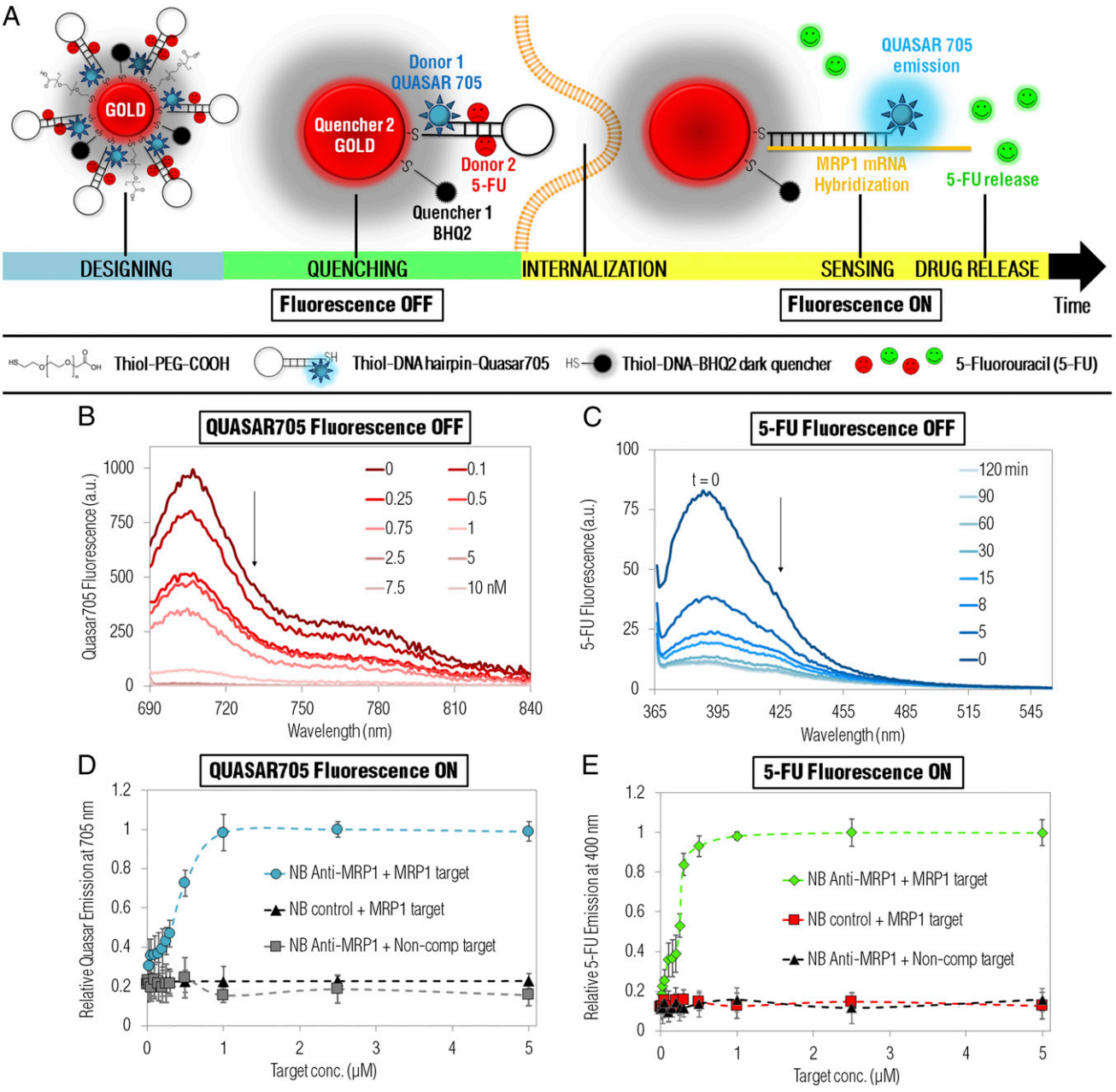

Fig. 1. Dark-gold nanobeacons designed to sense and overcome cancer multidrug resistance. (*A*) AuNPs (14 nm) functionalized with PEG, a thiol-DNA hairpin labeled with a NIR dye and a thiol-DNA oligo labeled with a dark quencher. These dark-gold nanobeacons are then loaded with 5-FU that intercalates in the beacon stem (dsDNA part) of the DNA hairpin oligo. Dark-gold nanobeacons are designed to silence the expression of *MRP1* and deliver at the same time the chemotherapeutic drug 5-FU, to circumvent essential MDR mechanisms. The AuNPs and the BHQ2 groups functioned as the quenchers and the Q705 and 5-FU as the donors. The fluorescence is OFF when the hairpin-DNA-Q705 is closed (i.e., no hybridization with the complementary target), and therefore no consequent 5-FU release occurs. The fluorescence is ON when the hairpin-DNA-Q705 hybridizes with a complementary target and an increase in Q705 emission occurs, with a concomitant 5-FU release and increase in the drug emission. (*B*) Fluorescent intensity change of Q705 (0.5 μM) after reaction with dark-gold nanobeacons at different concentration from 0 to 10 nM. Excitation wavelength = 675 nm. (*C*) Fluorescence emission spectra of 5-FU (1 mM) after incubation with 2.5 nM of dark-gold nanobeacons-Q705 for different periods of time (0–120 min). Q705 (*D*) and 5-FU (*E*) emission spectra after hybridization of nanobeacons anti-*MRP1* and nonsense with increasing amounts of the complementary and noncomplementary ssDNA target (0–5 μM).

after continuous exposure to drug compared with parental cancer cells (*SI Appendix*, Fig. S8).

Dark-gold nanobeacons could enter and accumulate in resistant MDA-MB-231 cells as verified by confocal microscopy, showing specific targeting at 48-h incubation of anti-Luc and anti-*MRP1* nanobeacons compared with nanobeacon nonsense (that do not hybridize with any target). It is evident that silencing occurs only with anti-Luc and anti-*MRP1* nanobeacons because hairpin conformational change due to specific hybridization to the target sequence can be identified via fluorescence emission (Fig. 2*A*). Epi-fluorescence images of cellular uptake kinetics of cells incubated with anti-*MRP1* nanobeacons for 0.5, 2, 4, 8, 24, and 48 h are depicted in *SI Appendix*, Fig. S9. Nanobeacons cellular uptake and detection associated with drug release signal for the same time points are depicted in *SI Appendix*, Fig. S10. Indeed, analytical flow cytometry data confirmed the phenomena observed via confocal imaging of a substantial increase in Quasar 705 signal only for nanobeacons anti-Luc and anti-*MRP1* compared with nanobeacon nonsense (Fig. 2*B*).

Confocal images of breast cancer cells further revealed that the dark-gold nanobeacons anti-*MRP1* were colocalized in intracellular organelles such as endosomes and/or lysosomes at 24 h and could escape out of this organelles at 48 h (Fig. 2*C*).

Overcoming Intracellular 5-FU Resistance. To corroborate confocal and flow cytometry data and overcome 5-FU resistance, resistant MDA-MB-231 cells were incubated with increasing amounts of dark-gold nanobeacons with and without 5-FU and evaluated by the live imaging system. As expected, only anti-Luc and anti-*MRP1* nanobeacons loaded with 5-FU can produce a substantial decrease in luminescence (Fig. 3*A*, also see *SI Appendix*, Fig. S11 for luminescence and fluorescence signal quantification). The same occurs for cell viability evaluated by MTT assay (Fig. 3 *B* and *C*). Dark-gold nanobeacons without 5-FU do not affect cell viability (Fig. 3*B*) compared with the dark-gold nanobeacons loaded with 5-FU, with an IC_{50} near 0.5 nM (Fig. 3*C*) at 72 h of exposure.

Live-dead staining of resistant MDA-MB-231 cells after uptake of increasing concentrations (0.1, 1, and 5 nM) of dark-gold nanobeacons for 48 h was performed using a double staining procedure with acridine orange (AO) and propidium iodide (PI) representing green and red fluorescence for live and dead cells, respectively. As shown in Fig. 3*D*, only nanobeacon anti-*MRP1* loaded with 5-FU (at 5 nM) results in extensive cell death (>95%), due to the combination of *MRP1* inhibition and consequent drug (5-FU) release. Nanobeacon anti-Luc shows modest cell death despite releasing the drug as *MRP1* inhibition does not occur (see *SI Appendix*, Fig. S12 for in vitro real-time PCR data) because *MRP1* can actively pump cytotoxic drugs like 5-FU

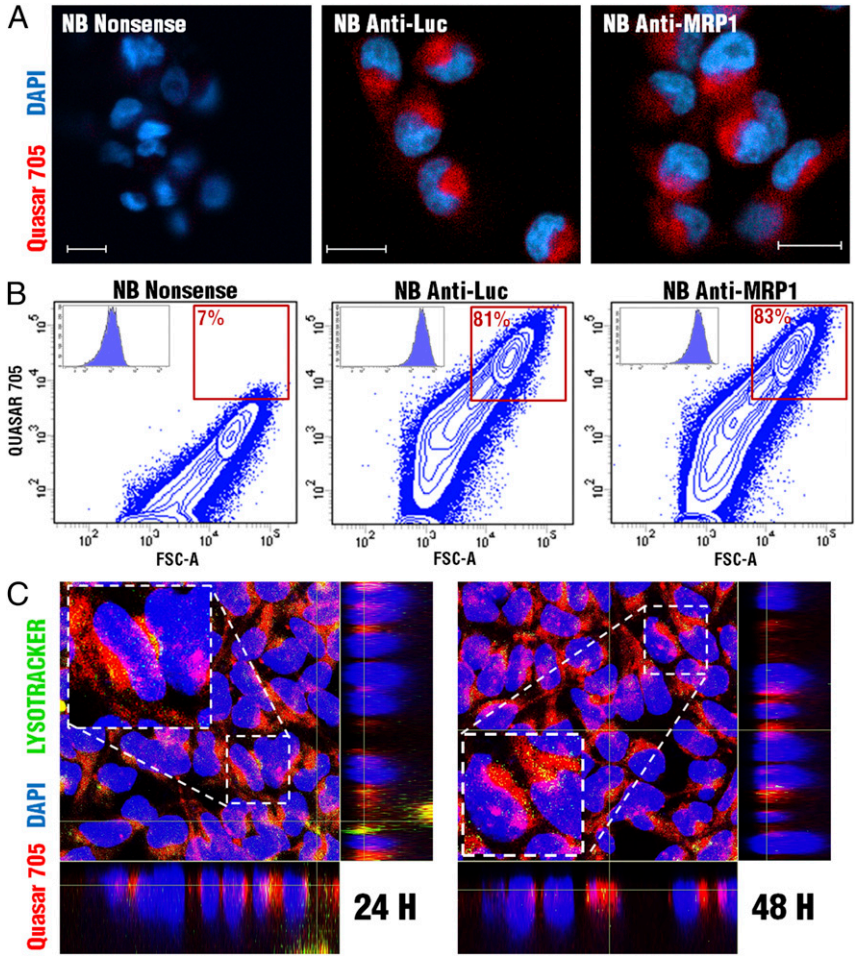

Fig. 2. (*A*) Representative confocal images of resistant MDA-MB-231 cells incubated for 48 h with a nanobeacon nonsense, nanobeacon anti-Luc, and nanobeacon anti-*MRP1* (5 nM). (Scale bars, 20 μm.) (*B*) Flow cytometry analysis comparing nanobeacon anti-Luc and nanobeacon anti-*MRP1*–treated cells to nanobeacon nonsense. (*C*) Intracellular colocalization of nanobeacon anti-*MRP1* within lysosomes. Resistant MDA-MB-231 cells were treated with 5 nM nanobeacon anti-*MRP1* (in red) for 24 and 48 h, and lysosomes (in green) were stained with Lysotracker Green DND26. Overlap of nanobeacon anti-*MRP1* and lysosome marker is represented in yellow in the merged images.

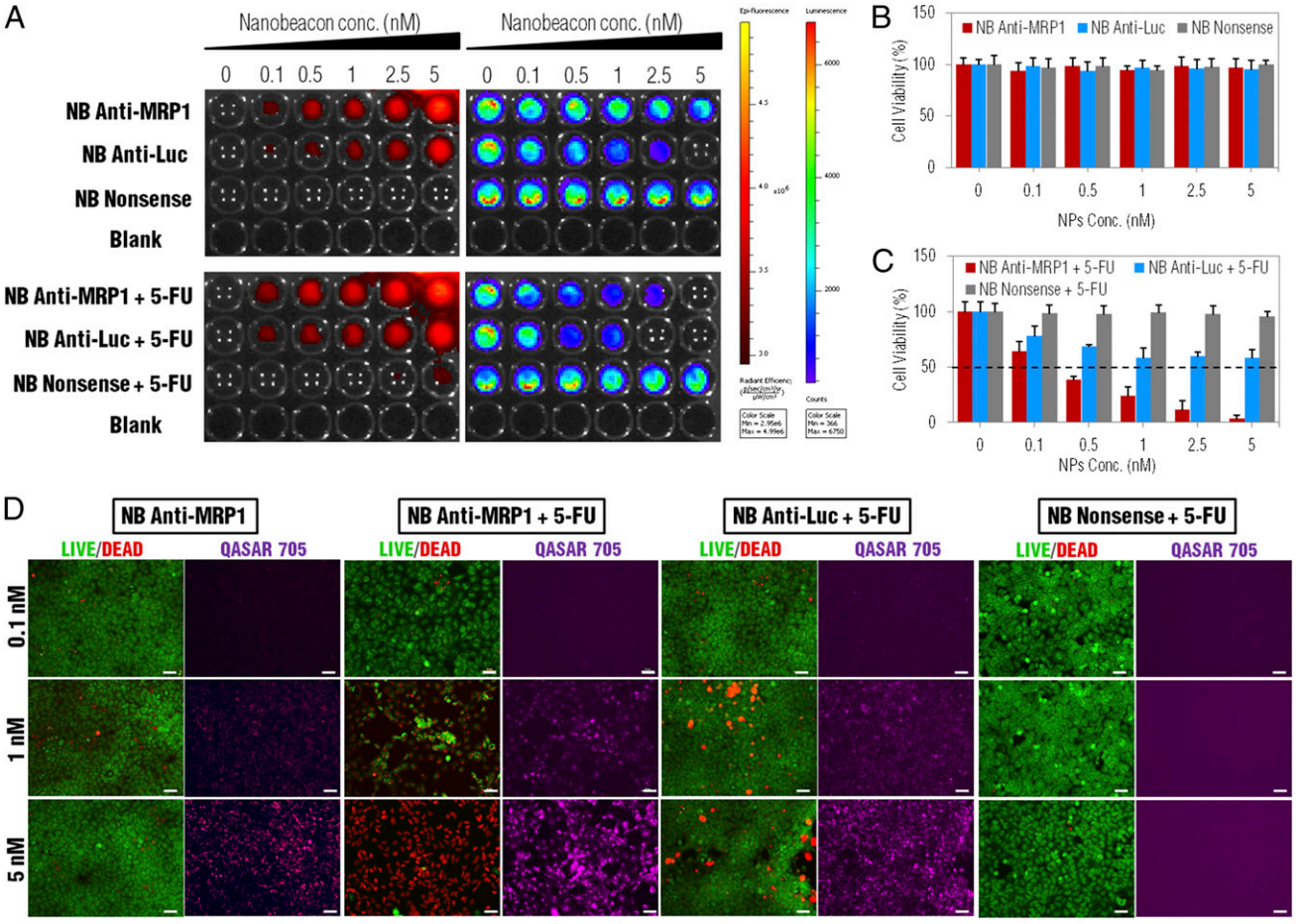

Fig. 3. (*A*) Fluorescence (in red) and luminescence signals of resistant MDA-MB-231 cells incubated with increasing amounts (0.1–5 nM) of dark-gold nanobeacons loaded without and with 5-FU. MTT assay of resistant MDA-MB-231 cells incubated for 72 h with increasing amounts of dark-gold nanobeacons without (*B*) and with (*C*) 5-FU. (*D*) Live-dead staining of resistant MDA-MB-231 tumor cells after uptake with 0.1, 1, and 5 nM of dark-gold nanobeacons (red, dead cells; green, live cells). (Scale bars, 25 μm.)

from the cytosol across the plasma membrane at the expense of ATP (28).

To evaluate the kinetics of the 5-FU effect and the mRNA *MRP1* knockdown by the nanobeacons, an MTT cell viability assay was performed after 24, 48, and 72 h and compared with the kinetics for *MRP1* expression using 5 nM (the same concentration for in vitro and in vivo studies) of nanobeacons loaded with 5-FU (*SI Appendix*, Fig. S13). These data corroborate that the maximum mRNA knockdown (at 48 h) occurs 24 h before the maximum effect of the drug (at 72 h), showing that the 5-FU is mostly effective 24 h after the drug reversal mechanism takes place.

Hydrogel-Gold Nanoswitch Sensing and Targeting in Vivo. To evaluate the efficiency of the dark-gold nanobeacon probes in sensing and in overcoming MDR in vivo, an orthotopic breast cancer mouse model was developed by injecting resistant MDA-MB-231 cells to the mammary fat pad of female SCID hairless congenic mice. Efficacious and local delivery of the dark-gold nanobeacon probes is achieved by the implantation of a hydrogel disk on top of the triple-negative breast tumors (Fig. 4*A*). The hydrogel scaffold comprising a polyamidoamine (PAMAM G5) dendrimer cross-linked with dextran aldehyde provides enhanced stability of the embedded nanoparticles. Epi-fluorescence images show a homogeneous distribution of the dark-gold nanobeacon probes (previously hybridized with a complementary target) in the hydrogel network (Fig. 4 *B* and *C*). The dual labeling discloses a colocalization of the nanobeacon probes (red) and the tagged polymeric matrix (green) that can be attributed to electrostatic interaction between the nanobeacons and the hydrogel (Fig. 4*C* and *SI Appendix*, Fig. S14). This reversible interaction enables rapid local release of the nanoparticles at the site of interest, as demonstrated by the almost complete release in the first 24 h under physiological conditions in vitro (pH 7.4 and 37 °C; *SI Appendix*, Fig. S15). This local delivery platform using dextran-dendrimer hydrogel scaffolds (29–31) overcomes some of the limitations associated with systemic administration, such as low stability, dissociation form vector, and short lifetimes (32). Additionally, local delivery prevents the uptake of systemically administered nanoparticles by the liver that makes targeting to other organs difficult. Once tumors reach a desired volume (~100 mm^3), hydrogel scaffolds loaded with dark-gold nanobeacon probes are implanted adjacent to the mammary fat pad tumor. Over a period of 14 d following hydrogel implantation, in vivo imaging was used to simultaneously track tumor inhibition as measured by luciferase expression (Fig. 4*D*), nanobeacon probes (Fig. 4*E*) before and after hybridization to *MRP1* mRNA, and hydrogel stability monitored by FITC fluorescence emission. No signs of inflammation were observed at the surgical site, and there were no changes in body weight following hydrogel implantation (*SI Appendix*, Fig. S16), suggesting that hydrogels are biocompatible, with no associated toxicity or side effects. Bioluminescence imaging of mice revealed that only nanobeacon anti-*MRP1* loaded with

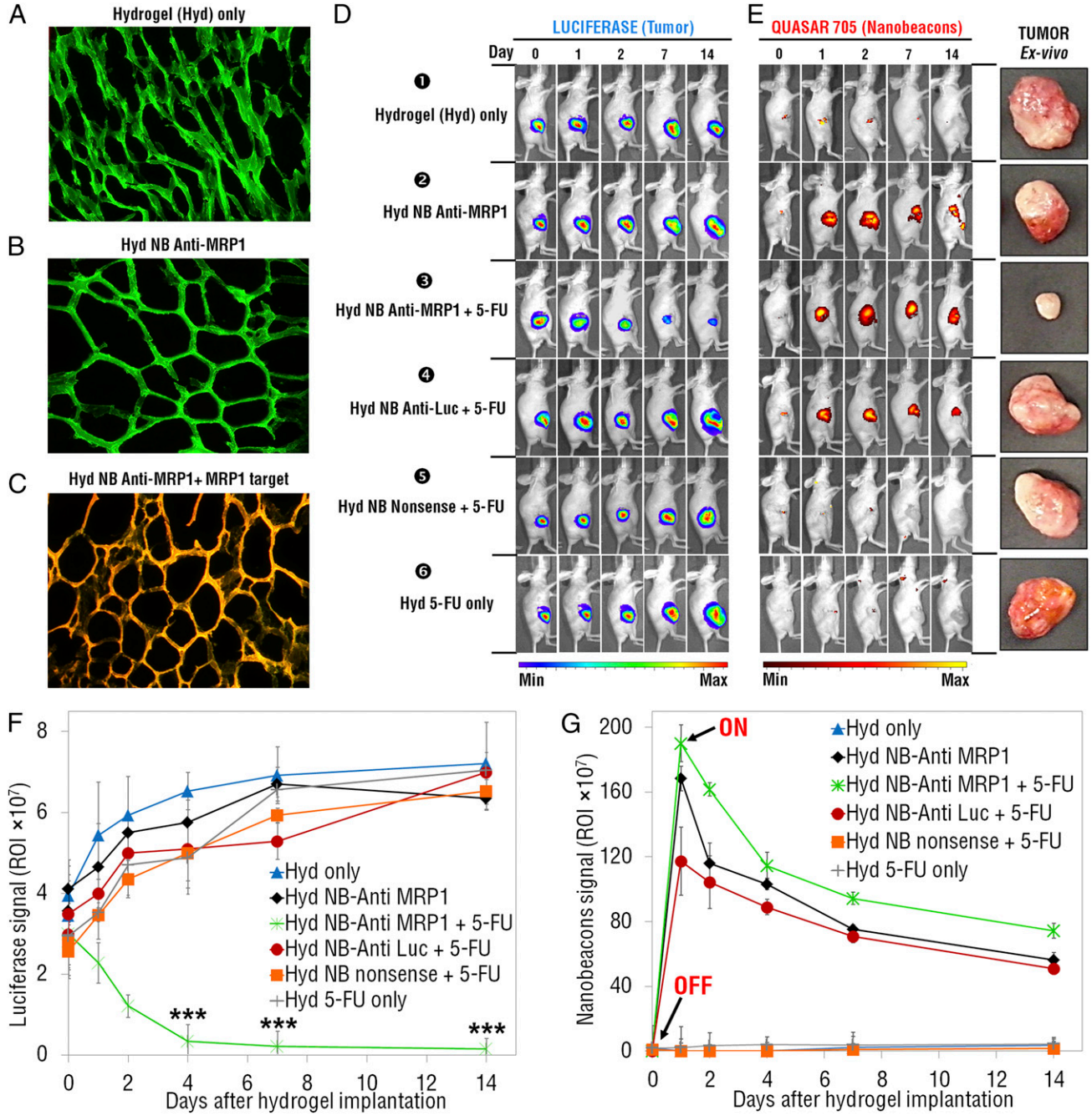

Fig. 4. Fluorescently labeled scaffolds loaded with dark-gold nanobeacons are implanted adjacent to the mammary fat pad tumor in mice. (*A*) Cryosection of dendrimer:dextran adhesive hydrogel (12 μm thickness) depicting adhesive morphology (dextran aldehyde was tagged with fluorescein). (*B*) Cryosection of anti-*MRP1* nanobeacon-doped dendrimer:dextran scaffold. (*C*) Cryosection of anti-*MRP1* nanobeacon (previously incubated with the complementary target *MRP1*)-doped dendrimer:dextran scaffold. Nanobeacons (red) are uniformly distributed in the hydrogel scaffold (green). (*D* and *E*) IVIS imaging of female SCID mice xenografted with triple-negative breast tumors implanted with hydrogels embedded with nanobeacon anti-*MRP1* with and without 5-FU, a nanobeacon anti-Luc with 5-FU, nanobeacon nonsense with 5-FU, and free drug (5-FU only). Representative imaging of individual mice from each treated group ($n = 5$ animals) is shown, with the same scale of photon flux indicating luciferase activity (*D*) and epi-fluorescence from the dark-gold nanobeacons Q705 signal (*E*). Ex vivo images of breast tumors for each group are also represented. (*F*) Evaluation of change in tumor size as a function of time after treatment with nanobeacons ($n = 5$, $^{***}P < 0.005$). (*G*) Nanobeacon probes (embedded in hydrogel) signal as a function of time after treatment with nanobeacons ($n = 5$, $^{***}P < 0.005$).

5-FU was able to promote efficient and sustained inhibition of tumor progression (Fig. 4*D*), with an ∼90% tumor size reduction 14 d after hydrogel disk implantation. Representative images of whole body organs and resected tumors in mice treated with nanobeacons are depicted in *SI Appendix*, Fig. S17, corroborating the significant tumor size reduction 14 d after hydrogel implantation. Interestingly, in vivo hydrogel degradation as monitored by FITC intensity (*SI Appendix*, Fig. S18) coincided with nanobeacon fluorescence, showing the highest signals during the first 2 d, in which the hydrogel degrades, and reaching about 45–50% degradation after 14 d.

Monitoring the change in tumor size as a function of time after treatment with nanobeacons revealed a significant reduction in

tumor growth ($n = 5$, $P < 0.005$) at day 14 after NP treatment (Fig. 4*F*), with almost complete tumor regression only for the nanobeacon anti-*MRP1* loaded with 5-FU group. About 90% decrease in luciferase activity (Fig. 4*F*) and in tumor size (*SI Appendix*, Fig. S17) was observed exclusively for the nanobeacon anti-*MRP1* loaded with 5-FU–treated tumors compared with free drug (5-FU only), anti-*MRP1* only, anti-Luc loaded with 5-FU, and nanobeacon nonsense with 5-FU ($n = 5$, $P < 0.005$). The free drug has no effect as expected because the cells are resistant to 5-FU. Only when we silence *MRP1* with the nanobeacon anti-*MRP1* does the drug become effective again. Concerning nanobeacon probe imaging, images of implanted hydrogels revealed that the fluorescent signal is OFF at day 0 (2 h after surgery) and is turned ON at day 1 (24 h), reaching a maximum intensity for *MRP1* and luciferase detection at day 2 (48 h) only for nanobeacon anti-*MRP1* with and without 5-FU and for nanobeacon anti-Luc loaded with 5-FU, respectively (Fig. 4*G*).

Ex Vivo Tumor Characterization and Biodistribution. Ex vivo organ biodistribution of nanobeacons at day 14 showed remarkable accumulation in the tumor (Fig. 5*A*), with no unspecific accumulation in the other main organs. In fact, ~40% of the nanobeacon probes persisted in the tumoral tissue (Fig. 5*A*). These data confirm the specificity of this platform in vivo, not only for sensing but specifically to overcome MDR in breast tumors. To confirm the observed in vivo effects, gene expression analysis of resected tumors was conducted to verify silencing of *MRP1*, as silencing of an important MDR gene would impart a substantially higher intracellular concentration of the chemotherapeutic drug. Indeed, real-time PCR results showed a decrease in *MRP1* expression in both nanobeacon anti-*MRP1* loaded with

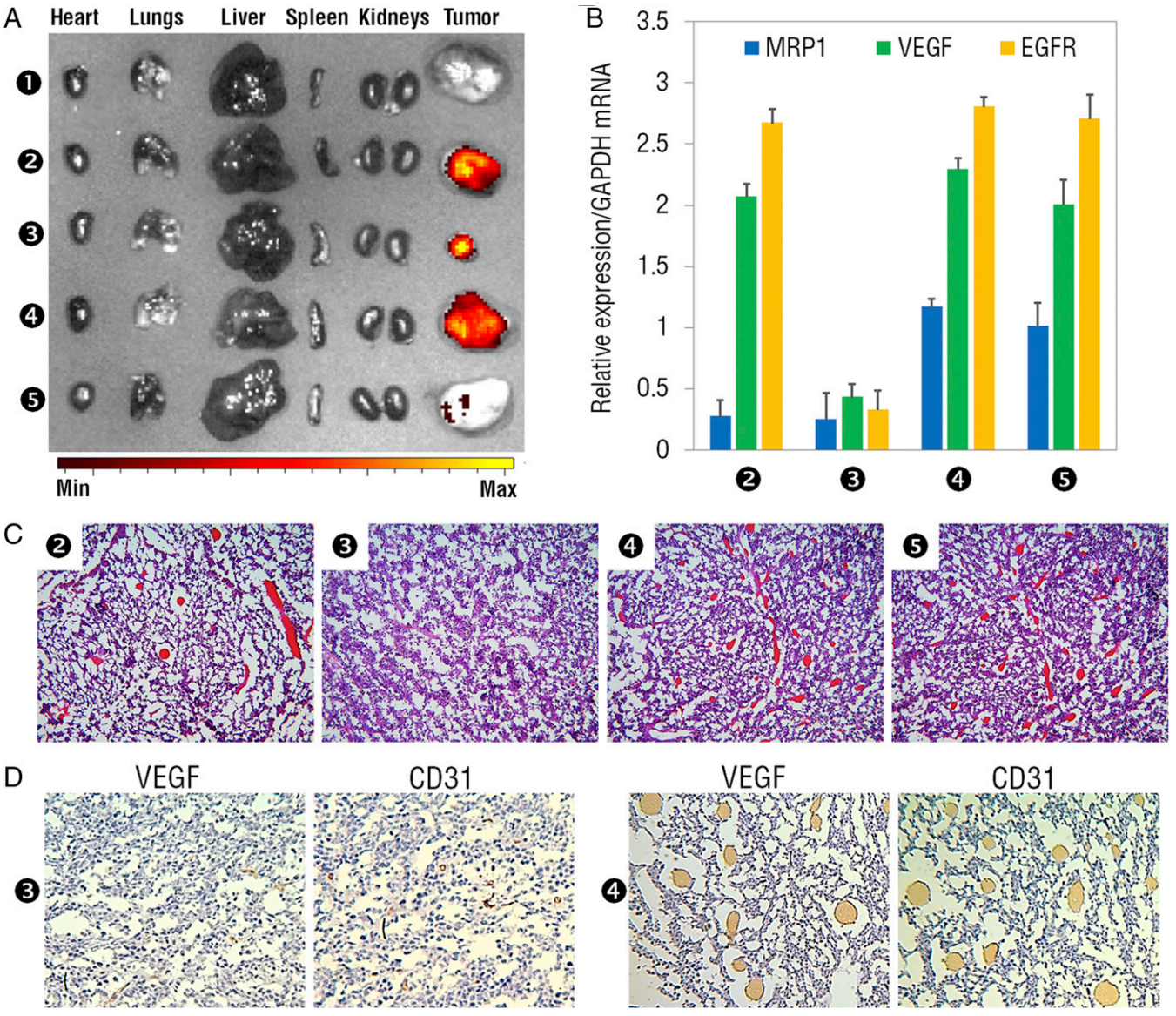

Fig. 5. (*A*) Epi-fluorescence images of whole body organs confirms selective accumulation of the dark-gold nanobeacons in tumors. (*B*) Evaluation of *MRP1*, VEGF, and EGFR expression via real-time PCR of tumors after treatment with nanobeacon anti-*MRP1* (❷), nanobeacon anti-*MRP1* with 5-FU (❸), nanobeacon anti-Luc with 5-FU (❹), and nanobeacon nonsense with 5-FU (❺), using GAPDH as the reference gene. (*C*) H&E stains of treated groups in hydrogels embedded with different nanobeacons, in mice bearing xenografts tumors. (*D*) Immunohistochemical evaluation of tumors treated with hydrogels embedded with nanobeacon anti-*MRP1* with 5-FU (❸) and with nanobeacon anti-Luc with 5-FU (❹) for VEGF and vessel density (CD31).

and without 5-FU. *MRP1* is a cell surface efflux pump involved in the redox regulation of MDR by reducing the intracellular concentration of 5-FU, making this a clinically relevant biomarker for triple-negative breast cancer. Nevertheless, expression of vascular endothelial growth factor (VEGF) and epidermal growth factor receptor (EGFR) decreases only after treatment with nanobeacon anti-*MRP1* loaded with 5-FU (Fig. 5*B*). H&E staining of breast tumor sections showed evidence of extensive reduction in vascularization for nanobeacon anti-*MRP1* loaded with 5-FU only (Fig. 5*C*), in accordance with tumor size reduction due to overcoming drug resistance. Immunohistochemical analysis showed that the expression of VEGF and the number of microvessels (CD31) were reduced only after treatment with hydrogels embedded with nanobeacon anti-*MRP1* with 5-FU (Fig. 5*D*). An increasing number of large vessels can be found in the control groups compared with nanobeacon anti-*MRP1* with 5-FU. The combination of specific tumor accumulation of these nanoparticles and their imaging properties represents an exciting opportunity for the simultaneous sensing and delivery of therapeutic agents for cancer gene therapy.

Outlook. Intrinsic or acquired multidrug resistance remains a major obstacle in the management of cancer. Therefore, a system capable of sensing and targeting MDR genes and able to overcome drug resistance is of utmost importance in cancer therapy. Injectable hydrogels placed adjacent to tumor surfaces have recently been developed and applied for RNAi silencing (29). Building on these advances, we designed an injectable hydrogel doped with gold nanobeacons as a smart ON/OFF molecular nanoswitch. This universal theranostics probe enables sensing and targeting of a specific multidrug resistance gene and selective delivery of a chemotherapeutic drug to triple-negative breast cancer tumors in vivo. The nanoswitch is ON only when detecting *MRP1* in the cell, a process that triggers concomitant drug release following nanobeacon opening. Silencing *MRP1* enables the reprogramming of resistant cancer cells to restore sensitivity to specific chemotherapeutic agents. A single application of this nanoswitch embedded in the hydrogels produced effective and sustained detection and gene silencing in breast tumors for at least 14 d with active drug release. Our nanodevice produces significant levels of gene knockdown and remarkable tumor size reduction. The approach taken in this study can be exploited to detect and inhibit any gene of interest in light of its endogenous expression in the tumor milieu, followed by the delivery of any choice of intercalated drug.

Materials and Methods

Synthesis of Bare-Gold Nanoparticles. Gold nanoparticles, with an average diameter of 13.8 ± 3.4 nm, were synthesized by the citrate reduction method described by Lee and Meisel (33). Briefly, 225 mL of 1 mM hydrogen tetrachloroaureate (III) hydrate (Sigma) (88.61 mg) was dissolved in 500 mL of distilled water, heated, and stirred under reflux. When the solution boiled, 25 mL of 38.8 mM sodium citrate dihydrate (Sigma; 285 mg) was added, resulting in a red solution. The solution was kept under ebullition with vigorous stirring and protected from light for 30 min. The solution was allowed to cool down and was kept protected from light. Bare-gold nanoparticles were characterized by TEM and UV-Vis molecular absorption spectra.

Synthesis of PEGylated-Gold Nanoparticles. Functionalization of PEGylated gold nanoparticles was carried out using commercial hetero-functional PEG functionalized with a 30% (wt/vol) saturated surface of α-mercapto-ω-carboxy PEG olution ($HS\text{-}C_2H_4\text{-}CONH\text{-}PEG\text{-}O\text{-}C_3H_6\text{-}COOH$; molecular weight, 3,500 Da; Sigma) as described elsewhere (34, 35). The 30% saturated PEG layer allows the incorporation of additional thiolated components, such as the thiolated DNA-hairpin-Quasar 705 nm and the tiolated-oligo-BHQ2 quencher. Briefly, 10 nM of the bare-gold nanoparticles was mixed with 0.006 mg/mL of PEG solution in an aqueous solution of SDS (0.028%). After this, the mixture was incubated for 16 h at room temperature. Excess PEG was removed by centrifugation (15,000 × *g*, 30 min, 4 °C) and quantified by a modification of the Ellman's Assay (see *SI Appendix* for complete protocol and quantification methods).

Synthesis of Dark-Gold Nanobeacons. We prepared three different sequences of gold nanobeacons: a nanobeacon anti-*MRP1* (detects and inhibits *MRP1* mRNA), a nanobeacon anti-Luc (internal control, hybridizes with luciferase mRNA and releases the drug; however, does not target *MRP1*), and a nanobeacon nonsense (designed to not hybridize with any target within the genome; *SI Appendix*, Table S1 for thiol-DNA-hairpin Quasar705 sequences). All of these nanobeacons were also functionalized with a DNA-oligo-BHQ2 dark quencher. Briefly, the thiolated oligonucleotides (Sigma)—thiol-DNA-hairpin Quasar705 and DNA-oligo-BHQ2 dark quencher—were suspended in 1 mL of 0.1 M DTT (Sigma), extracted three times with ethyl acetate, and further purified through a desalting NAP-5 column (GE Healthcare) using 10 mM phosphate buffer (pH 8) as eluent. Following oligonucleotide quantification via UV/Vis spectroscopy, each oligomer was added to the AuNP-PEG solution in a 50:1 ratio. AGE I solution [2% (wt/vol) SDS, 10 mM phosphate buffer (pH 8)] was added to the mixture to achieve a final concentration of 10 mM phosphate buffer (pH 8), 0.01% (wt/vol) SDS. The solution was sonicated for 10 s using an ultrasound bath and incubated at room temperature for 20 min. Afterward, the ionic strength of the solution was increased sequentially in 50 mM NaCl increments by adding the required volume of AGE II solution [1.5 M NaCl, 0.01% (wt/vol) SDS, 10 mM phosphate buffer (pH 8)] up to a final concentration of 10 mM phosphate buffer (pH 8), 0.3 M NaCl, 0.01% (wt/vol) SDS. After each increment, the solution was sonicated for 10 s and incubated at room temperature for 20 min before the next increment. Following the last addition, the solution was left to rest for additional 16 h at room temperature. Then, the functionalized dark-gold nanobeacons were centrifuged for 20 min at 15,000 × *g*, and the oily precipitate was washed three times with MilliQ water and redispersed in MilliQ water. The resulting dark-gold nanobeacons were stored in the dark at 4 °C until further use. Characterization of the dark-gold nanobeacons was performed by DLS (Wyatt Dyna Pro Plate Reader), UV/Vis spectroscopy, and TEM (*SI Appendix*, Table S2).

Stability and Specificity Assays for Dark-Gold Nanobeacons. For the detection of specific targets, 2.5 nM of nanobeacon anti-*MRP1* and nanobeacon nonsense in 10 mM of phosphate buffer, pH 7, was added to 5 nM of complementary *MRP1* target (Sigma). All measurements were performed in a microplate reader (Varioskan Flash Multimode Reader; Thermo Scientific) programmed to incubate the reactions for 120 min at 37 °C while recording the fluorescence intensity every 2 min at an excitation wavelength of 675 nm for Quasar705-labeled gold nanobeacon and at an excitation of 350 nm for 5-FU. To evaluate whether the reductive cell environment would cause detachment of the thiol-DNA hairpin from the dark-gold nanobeacons, resistance to intracellular concentrations of GST was studied. To mimic the behavior in the intracellular milieu, 2.5 nM of the nanobeacon anti-*MRP1* was incubated with 0.1, 1, 5 (physiological concentration), 10, and 100 mM GST (Sigma) at 37 °C for up to 120 min, measuring fluorescence intensity every 2 min (Exc/Emi = 675/705 nm for Quasar705-labeled gold nanobeacon; Exc/Emi = 350/400 nm for 5-FU). The same procedure described above was performed for stability at different pHs (4.5, 5.5, 6.5, 7, 7.5, and 8), different temperatures (25 °C, 37 °C, 42 °C, and 45 °C), and different DNase concentrations (0.5, 1, 2.5, and 5 U).

In Vitro Dark-Gold Nanobeacon's Delivery. MDA-MB-231 cells (from triple-negative breast cancer) were grown in DMEM (Invitrogen) supplemented with 4 mM glutamine, 10% heat inactivated FBS (Invitrogen), 100 U/mL penicillin, and 100 μg/mL streptomycin (Invitrogen) and maintained at 37 °C in 5% CO_2. Cells were seeded at a density of 1×10^5 cells per well in 24-well plates and grown for 24 h before incubation with nanobeacons. On the day of incubation, the cells were ∼50% confluent. An MDR breast cancer cell line MDA-MB-231 was also developed by continuous culture of parental MDA-MB-231 cells in 5-FU and maintained with 5-FU at a dose of 0.05 mg/mL for 6 wk. After 6 wk, drug resistance was achieved, as was evident by the absence of cell death via an MTT assay after continuous exposure to drug compared with parental cancer cells. Briefly, a standard MTT reduction assay was performed to determine the resistance status of the cells and the cytotoxicity of the gold nanobeacons. Cells were seeded at a density of 1×10^5 cells per well in 24-well culture plates in complete DMEM (500 μL) with serum. After 24 h of exposure, the medium was removed, the cells were washed twice with sterile PBS, and 300 μL of fresh medium with serum was added. Then 16.7 μL of sterile MTT stock solution (5 mg/mL in PBS) was added to each well. After incubation for an additional 2 h, the medium was removed, and the formazan crystals were resuspended in 300 μL of dimethyl sulfoxide (Sigma). The solution was mixed, and its absorbance was measured at 540 nm as a working wavelength and 630 nm as reference using a microplate reader (Varioskan Flash

Multimode Reader; Thermo Scientific). The cell viability was normalized to that of cells cultured in the culture medium with PBS treatment. The viability of cells was also visualized by using a double staining procedure with AO (green, live cells) and PI (red, dead cells). Briefly, 0.5 mL of complete medium containing 0.67 μM AO and 75 μM PI was added to each well and was incubated in the dark at 37 °C for 30 min. After rinsing with fresh medium, live and dead cells were monitored using a fluorescence microscope (Nikon Eclipse Ti). For confocal microscopy, cells were fixed with 4% (wt/vol) paraformaldehyde in PBS for 15 min at 37 °C and mounted in ProLong Gold Antifade Reagent with DAPI (Invitrogen) to allow for nuclear staining. Images of cells were taken with a Nikon A1R Ultra-Fast Spectral Scanning Confocal Microscope.

Flow Cytometry. MDA-MB-231 cells incubated with Q705 dark gold nanobeacons were analyzed, and data were acquired by FACS LSR HTS-2 (BD Biosciences) flow cytometer.

Quantitative PCR. Total RNA from MDA-MB-231 cells and breast tumors from SCID mice was extracted using the RNeasy Plus Mini Kit (Qiagen) according to the manufacturer's protocol. cDNA was produced using a High-Capacity cDNA Reverse Transcription Kit (Applied Biosystems) using 500 ng of total RNA. Quantitative RT-PCR was performed with Taqman probes FAM-MGB for *MRP1* (ABCC1) and GAPDH (Applied Biosystems). GAPDH was used as a reference gene. The reactions were processed using Light Cycler 480 II Real-time PCR machine (Roche) using TaqMan Gene Expression Master Mix (Applied Biosystems) under the following cycling steps: 2 min at 50 °C for uracil *N*-glycosylase (UNG) activation; 10 min at 95 °C; 40 cycles at 95 °C for 15 s; and 60 °C for 60 s. At least three independent repeats for each experiment were carried out. Gene expression was determined as a fold difference after normalizing to the housekeeping gene GAPDH.

Development of Orthotopic Triple-Negative Breast Cancer Mouse Model. Tumors in the mammary fat pad were induced in female SCID hairless congenic mice by injection of 5×10^6 resistant MDA-MB-231 cells stably expressing firefly luciferase, suspended in 50 μL of Hank's balanced salt solution (HBSS; Lonza). For determination of tumor growth, individual tumors were measured via caliper, and tumor volume was calculated by tumor volume (mm^3) = width × [length(2)]/2. Treatments began when tumor volume reached about 100 mm^3. All experimental protocols were approved by the Massachusetts Institute of Technology Animal Care and Use Committee and were in compliance with National Institutes of Health guidelines for animal use.

Hydrogel-Dark-Gold Nanobeacon Synthesis and in Vivo Implantation. Dextran aldehyde was tagged by reaction with fluorescein thiosemicarbazide (Invitrogen) in 20 mL of 0.1 M phosphate buffer (pH 7.5) for 30 min at room temperature. Then, the reaction crude was cooled down in an ice-water bath, and imine bonds were reduced with 20 mL of 30 mM sodium cyanoborohydrate in PBS for 30 min. Tagged dextran aldehyde was dialyzed against double distilled water using a 10,000-Da molecular cutoff filter for 8 d and lyophilized. Tagged hydrogel scaffolds were developed as previously described (36). Briefly, equal parts of PAMAM G5 dendrimer (Dendritech) amine of 12.5% (wt/vol) solid content and dextran aldehyde 5% (wt/vol) solid content with 0.25% fluorescently labeled dextran were mixed to form 6-mm precured disks. For doped scaffolds, nanobeacons were added to the dendrimer solution before hydrogel formation at a concentration of 20 nM. All solutions were filtered through a 0.22-μm filter before hydrogel formation for in vivo implantation. Precured disks of fluorescently labeled scaffold with or without nanobeacons were formed and implanted peritumorally in SCID mice.

Hydrogel-Dark-Gold Nanobeacon Fluorescence Imaging. Precured fluorescently labeled scaffolds alone (control), doped with nonhybridized and hybridized nanobeacons, were snap-frozen in liquid nitrogen and kept at −80 °C for 24 h. Then, 12-μm-thick cryosections (Cryostat Leica CM1850) were analyzed by fluorescence microscopy (NIS-Elements Nikon).

Dark-Gold Nanobeacon Stability in Vitro. Nanobeacons (final concentration, 5 nM) were pretreated with and without complementary target *MRP1* and incubated at 37 °C in dextran and dendrimer solutions [final concentrations of 5% (wt/vol) and 12.5% (wt/vol) in water, respectively]. Samples were collected at different time points, and fluorescence was measured (Varioskan Flash Multimode Reader; Thermo Scientific). Fluorescence intensity was plotted over time.

Hydrogel-Dark-Gold Nanobeacon Release in Vitro. Precured disks of fluorescently labeled hydrogel scaffold doped with hybridized nanoparticles were incubated in PBS at 37 °C. At different time points, samples were collected from the PBS, and the fluorescence of released products was quantified (Varioskan Flash Multimode Reader; Thermo Scientific). Data were plotted as percent nanobeacons/dextran aldehyde released for each time point. Controls for this experiment included scaffold without nanobeacons and scaffold with nonhybridized nanobeacons.

Analysis of Tumor Growth and Hydrogel-Gold Nanobeacon Degradation. Noninvasive longitudinal monitoring of tumor progression was followed by the luminescent signal from the MDA-MB-231 cells ($n = 5$ animals per treated group) using IVIS Spectrum imaging system (Xenogen XMP-2 Corporation). Fifteen minutes before imaging, mice were administered with 150 μL of D-luciferin (30 mg/mL; Perkin-Elmer) in Dulbecco's phosphate-buffered saline (DPBS) via i.p. injection. Whole-animal imaging was performed at the indicated time points: days 0 (2 h after gel implantation), 1, 2, 4, 7, and 14. Assessment of in vivo toxicity via mice body weight evaluation was performed on all of the animal groups for 37 d after hydrogel-gold nanobeacon exposure.

Statistics. Differences between groups were examined using the Student paired *t* test through the SPSS statistical package (version 17; SPSS Inc.). All error bars used in this report are mean ± SD of at three independent experiments. All in vivo experiments used five mice per treatment group unless noted otherwise.

ACKNOWLEDGMENTS. We thank the Peterson Nanotechnology Materials Core Facility and the Swanson Biotechnology Center at the Koch Institute for Integrative Cancer Research at Massachusetts Institute of Technology (MIT) for assistance with animal experiments and facilities, especially the microscopy, flow cytometry, and histology cores. We thank the Department of Comparative Medicine, MIT, especially Dr. Jennifer Haupt. We thank Dr. Glenn Paradis for FACS assistance with Cancer Center Support (FACS core) Grant P30-CA14051 from the National Cancer Institute. J.C. acknowledges Marie Curie International Outgoing Fellowship and Funding (FP7-PEOPLE-2013-IOF, Project 626386).

1. Gottesman MM, Fojo T, Bates SE (2002) Multidrug resistance in cancer: Role of ATP-dependent transporters. *Nat Rev Cancer* 2(1):48–58.
2. Higgins CF (2007) Multiple molecular mechanisms for multidrug resistance transporters. *Nature* 446(7137):749–757.
3. Munoz M, Henderson M, Haber M, Norris M (2007) Role of the MRP1/ABCC1 multidrug transporter protein in cancer. *IUBMB Life* 59(12):752–757.
4. Choi CH (2005) ABC transporters as multidrug resistance mechanisms and the development of chemosensitizers for their reversal. *Cancer Cell Int* 5:30.
5. Nooter K, de la Riviere GB, Klijn J, Stoter G, Foekens J (1997) Multidrug resistance protein in recurrent breast cancer. *Lancet* 349(9069):1885–1886.
6. Nolè F, et al. (2001) Vinorelbine, cisplatin and continuous infusion of 5-fluorouracil (ViFuP) in metastatic breast cancer patients: A phase II study. *Ann Oncol* 12(1): 95–100.
7. Giacchetti S, et al. (2000) Phase III multicenter randomized trial of oxaliplatin added to chronomodulated fluorouracil-leucovorin as first-line treatment of metastatic colorectal cancer. *J Clin Oncol* 18(1):136–147.
8. Conde J, de la Fuente JM, Baptista PV (2013) Nanomaterials for reversion of multidrug resistance in cancer: A new hope for an old idea? *Front Pharmacol* 4:134.
9. Conde J, Edelman ER, Artzi N (2015) Target-responsive DNA/RNA nanomaterials for microRNA sensing and inhibition: The jack-of-all-trades in cancer nanotheranostics? *Adv Drug Deliv Rev* 81C:169–183.
10. Li C (2014) A targeted approach to cancer imaging and therapy. *Nat Mater* 13(2): 110–115.
11. Conde J, Bao C, Cui D, Baptista PV, Tian F (2014) Antibody-drug gold nanoantennas with Raman spectroscopic fingerprints for in vivo tumour theranostics. *J Control Release* 183:87–93.
12. Schroeder A, et al. (2012) Treating metastatic cancer with nanotechnology. *Nat Rev Cancer* 12(1):39–50.
13. Conde J, et al. (2013) In vivo tumor targeting via nanoparticle-mediated therapeutic siRNA coupled to inflammatory response in lung cancer mouse models. *Biomaterials* 34(31):7744–7753.
14. Mura S, Nicolas J, Couvreur P (2013) Stimuli-responsive nanocarriers for drug delivery. *Nat Mater* 12(11):991–1003.
15. Irvine DJ (2011) Drug delivery: One nanoparticle, one kill. *Nat Mater* 10(5):342–343.
16. Conde J, Doria G, Baptista P (2012) Noble metal nanoparticles applications in cancer. *J Drug Deliv* 2012:751075.

17. Gil PR, Parak WJ (2008) Composite nanoparticles take aim at cancer. *ACS Nano* 2(11): 2200–2205.
18. Dong X, Mumper RJ (2010) Nanomedicinal strategies to treat multidrug-resistant tumors: Current progress. *Nanomedicine (Lond)* 5(4):597–615.
19. Patel NR, Pattni BS, Abouzeid AH, Torchilin VP (2013) Nanopreparations to overcome multidrug resistance in cancer. *Adv Drug Deliv Rev* 65(13-14):1748–1762.
20. Markman JL, Rekechenetskiy A, Holler E, Ljubimova JY (2013) Nanomedicine therapeutic approaches to overcome cancer drug resistance. *Adv Drug Deliv Rev* 65(13-14): 1866–1879.
21. Liedtke C, et al. (2008) Response to neoadjuvant therapy and long-term survival in patients with triple-negative breast cancer. *J Clin Oncol* 26(8):1275–1281.
22. Conde J, et al. (2014) Gold-nanobeacons for gene therapy: Evaluation of genotoxicity, cell toxicity and proteome profiling analysis. *Nanotoxicology* 8(5):521–532.
23. Rosa J, Conde J, de la Fuente JM, Lima JC, Baptista PV (2012) Gold-nanobeacons for real-time monitoring of RNA synthesis. *Biosens Bioelectron* 36(1):161–167.
24. Conde J, Rosa J, de la Fuente JM, Baptista PV (2013) Gold-nanobeacons for simultaneous gene specific silencing and intracellular tracking of the silencing events. *Biomaterials* 34(10):2516–2523.
25. Rakoczy PE (2001) Antisense DNA technology. *Methods Mol Med* 47:89–104.
26. Mu CJ, Lavan DA, Langer RS, Zetter BR (2010) Self-assembled gold nanoparticle molecular probes for detecting proteolytic activity in vivo. *ACS Nano* 4(3):1511–1520.
27. Griffin J, et al. (2009) Size- and distance-dependent nanoparticle surface-energy transfer (NSET) method for selective sensing of hepatitis C virus RNA. *Chemistry* 15(2): 342–351.
28. Faneyte IF, Kristel PMP, van de Vijver MJ (2004) Multidrug resistance associated genes MRP1, MRP2 and MRP3 in primary and anthracycline exposed breast cancer. *Anticancer Res* 24(5A):2931–2939.
29. Segovia N, et al. (2015) Hydrogel doped with nanoparticles for local sustained release of siRNA in breast cancer. *Adv Healthc Mater* 4(2):271–280.
30. Artzi N, Shazly T, Baker AB, Bon A, Edelman ER (2009) Aldehyde-amine chemistry enables modulated biosealants with tissue-specific adhesion. *Adv Mater* 21(32-33):3399–3403.
31. Artzi N, et al. (2011) In vivo and in vitro tracking of erosion in biodegradable materials using non-invasive fluorescence imaging. *Nat Mater* 10(9):704–709.
32. Wolinsky JB, Colson YL, Grinstaff MW (2012) Local drug delivery strategies for cancer treatment: Gels, nanoparticles, polymeric films, rods, and wafers. *J Control Release* 159(1):14–26.
33. Lee PC, Meisel D (1982) Adsorption and surface-enhanced Raman of dyes on silver and gold sols. *J Phys Chem* 86(17):3391–3395.
34. Sanz V, et al. (2012) Effect of PEG biofunctional spacers and TAT peptide on dsRNA loading on gold nanoparticles. *J Nanopart Res* 14(6):1–9.
35. Conde J, et al. (2012) Design of multifunctional gold nanoparticles for in vitro and in vivo gene silencing. *ACS Nano* 6(9):8316–8324.
36. Oliva N, et al. (2012) Natural tissue microenvironmental conditions modulate adhesive material performance. *Langmuir* 28(43):15402–15409.